Journal of the Physical Society of Japan
Vol. 68, No. 9, September, 1999, pp. 3100-3109

Local and Nonlocal Excitations in Cu $4p$-$1s$ Resonant X-Ray Emission Spectra of Nd_2CuO_4

Tsuyoshi IDÉ* and Akio KOTANI

Institute for Solid State Physics, the University of Tokyo, 7-22-1 Roppongi, Minato-ku, Tokyo 106-8666

(Received April 12, 1999)

Theoretical study for Cu $4p$-$1s$ resonant X-ray emission spectroscopy (RXES) of Nd_2CuO_4 is given in the context of local and nonlocal natures of electronic excitations. Detailed analyses with an impurity Anderson model and multi-Cu models are presented, based on exact diagonalization technique. By investigating partial densities of states, basic characters of each excited state are clarified. It is demonstrated that a disagreement with experimental data is unavoidable with the impurity model. The key concept to solve the difficulty is Zhang-Rice singlet formation in the intermediate state of RXES. We find that it survives in the final state of RXES as the lowest charge-transfer excitation. The limitation of the impurity model and the essential role of nonlocal excitations in RXES are stressed.

KEYWORDS: insulating cuprates, Zhang-Rice singlet, resonant X-ray emission, Cu $1s$-$4p$ excitation, multi-site cluster, charge-transfer gap, Lanczos method

§1. Introduction

Recent progress in synchrotron radiation technique has opened up a new way to investigate complicated electronic systems. Resonant X-ray emission spectroscopy (RXES) is one of the most promising ones. Several experimental studies on strongly correlated electron systems with RXES have been performed, for instance, for Ti,[1,2] Mn[3] and Ni[4] oxides. In contrast to the first-order optical process such as X-ray photoemission spectroscopy (XPS) or X-ray absorption spectroscopy (XAS), there is no deep core hole in the final state. Thereby their itinerant nature should be reflected on the spectra, despite of the site-selectivity. A recent theoretical study of the present authors suggests that a nonlocal kind of excitations is a key concept to explain the spectral shapes.[5]

The Cu $4p_\pi$-$1s$ RXES of Nd_2CuO_4 has recently been measured by Hill and coworkers.[6] Nd_2CuO_4 is well known as a mother material of n-type superconductor, $Nd_{2-x}Ce_xCuO_{4-y}$,[7] which has attracted special attention in the context of appearance of the electron-hole symmetry,[8] a character which single-band models should have. Nd_2CuO_4 has two-dimensional (2D) corner-shared CuO_2 plane with nominally d^9 configuration, which is believed to be essential for high-T_C superconductivity. The Cu $4p$-$1s$ RXES process is schematically shown in Fig. 1. A completely localized $1s$ core electron is resonantly excited to an empty $4p$ conduction band by an incident photon ($\sim$ 9 keV), and then the excited $4p$ electron radiatively comes back to the $1s$ core orbital. In the intermediate state (Fig. 1(b)), a valence hole on the core hole site is strongly scattered to move away to surrounding sites, so that the dynamics of the "dopant" hole such as Zhang-Rice (ZR) singlet formation[9] would be strongly reflected on the RXES spectra. It is interesting to see how the ZR singlet state decays or survives with going to the final states, and to examine what kind of state is created above the insulating gap through varying the incident photon energy.

Figure 2 shows the experimental data of the Cu $4p_\pi$-$1s$ RXES of Nd_2CuO_4.[6] The abscissa is the energy loss of X-ray, which is the same as the energy difference between the final and initial electronic states. The inci-

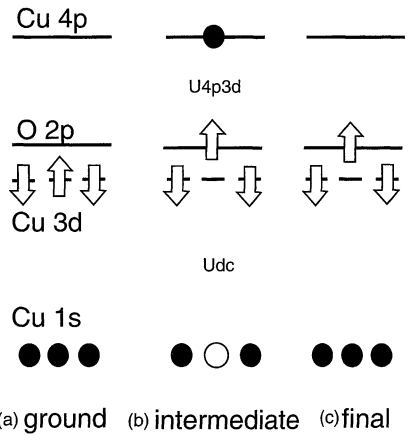

Fig. 1. Schematic diagram of Cu $1s$-$4p$-$1s$ RXES process. The blank circle and blank arrows represent a $1s$ core hole and up- or down-spin valence holes, respectively. The shaded circles represent $1s$ or $4p$ electrons. (a) Ground state with antiferromagnetic order. (b) Intermediate state, where a photon excited a $1s$-electron to an empty $4p$ level (the $4p$ band width is disregarded in this figure), creating a $1s$ core hole. The strong repulsive interaction U_{dc} between $3d$ and $1s$ holes gives rise to a charge-transfer (CT) excitation. There is also attractive interaction U_{4p3d} between $4p$ electron and $3d$ hole, but it can not completely compensate U_{dc}. (c) A final state with the CT excitation. The energy difference between the final and ground states is observed as energy loss of the X-ray.

* E-mail: ide@kodama.issp.u-tokyo.ac.jp

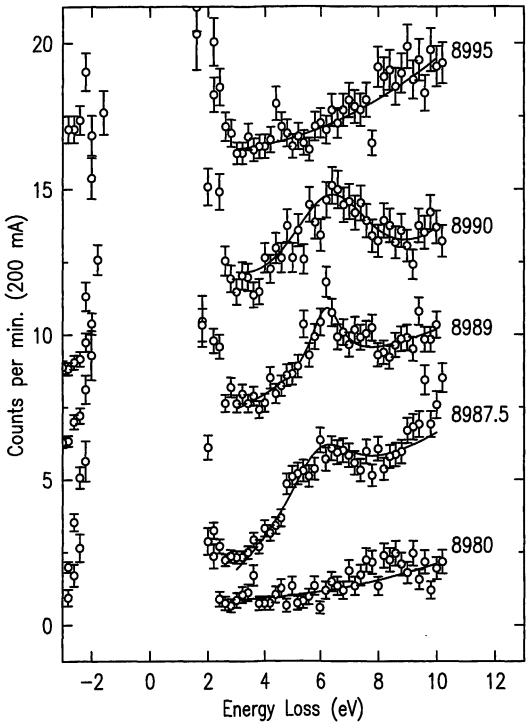

Fig. 2. Cu $4p_\pi$-$1s$ RXES of Nd_2CuO_4[6] as a function of energy loss $E_f - E_g$. Incident photon energies are in the range of $1s$-$4p_\pi$ absorption. The polarization vector of the incident X-ray has an angle 60° to CuO_2 plane, and its momentum-transfer is perpendicular to that. The excitation energies are indicated in the upper panels of Fig. 3 with vertical bars.

dent photon energy is taken in the region of Cu $1s$-$4p_\pi$ XAS, which is shown in the upper panel of Fig. 3(a) with the open circles. The first (at 8984 eV) and second (at 8990 eV) features of the Cu $1s$-$4p_\pi$ XAS are denoted by a main peak and a satellite, respectively. It is seen in Fig. 2 that an inelastic structure at about 6 eV is observed for 8987.5, 8989 and 8990 eV in addition to the extremely strong elastic peak at zero. The incident photon energy dependence of the 6 eV excitation is shown in the lower panel of Fig. 3(a) with the open circles. We recognize that the 6 eV intensity is strongly enhanced when the incident photon energy is tuned at the satellite of the XAS, but it indicates almost *no* enhancement at the main peak position.

The aim of this paper is to give a theoretical interpretation for these experimental data. We will first analyze the experimental data with an impurity Anderson model. The calculated results will be in fair agreement with the experiment, but there exists a conspicuous difference between the theoretical and exper imental results: The calculated 6 eV intensity shows a considerable enhancement at the main peak position. In order to remove this discrepancy, we will next use a multi-Cu cluster model. It will be shown that the 6 eV intensity is strongly suppressed at the main peak resonance because of the formation of a ZR singlet in the intermediate state. To the authors' knowledge. this is the first quantitative analysis of experimental RXES spectra based on "large" cluster models.

The layout of the present paper is as follows: In the

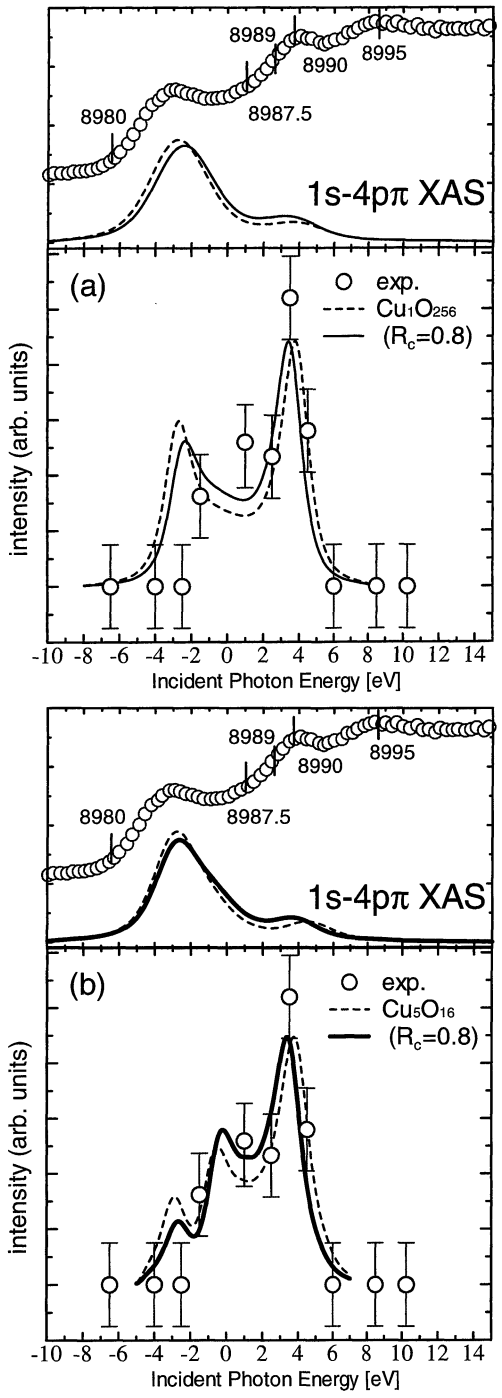

Fig. 3. (a) Lower panel: the 6 eV intensity as a function of the incident photon energy in Cu $4p_\pi$-$1s$ RXES of Nd_2CuO_4. The open circles represent the experimental result by Hill *et al.*[6] The solid and dashed curves represent calculated results with a Cu_1O_{256} cluster (impurity Anderson model), where solid and dashed ones show the results with $R_c = 0.8$ and 1.0, respectively. In accordance with the experimental resolution,[6] all the calculations are convoluted with Gaussian $\Gamma_G = 0.95$ eV (HWHM) for scattered photon, and $\Gamma_G = 0.3$ eV for incident photon. Upper panel: the open circles represent experimental Cu K-XAS of Nd_2CuO_4,[10] where the polarization vector of the X-ray is 60° to the CuO_2 plane. The definition of the two curves are the same as the lower panel, although they are convoluted with Lorentzian $\Gamma_L = 0.8$ eV (HWHM) to take in lifetime effects, and further with $\Gamma_G = 0.8$ eV to reproduce the experimental line width. (b) Lower panel: the same as that of (a), but calculated curves are obtained with a multi-Cu Cu_5O_{16} cluster. Upper panel: the same as that of (a), but calculated curves are obtained with a multi-Cu Cu_5O_{16} cluster, which are broadened with $\Gamma_L = 0.8$ eV and $\Gamma_G = 1.2$ eV.

next section, the models used are explained. Numerical analysis with the impurity Anderson model is described in § 3. We discuss in § 4 the role of the nonlocal screening effects with multi-Cu cluster models. In the last section a brief summary of the present study is given.

§2. Formulation

2.1 Hamiltonian

We consider a 2D extended d-p model with corner-shared structure, as shown in Fig. 4. The explicit form of the Hamiltonian is as follows:

$$H = H_{dp} + H_{dd} + H_{pp} + H_{\rm core} + H_{dc} + H_{4p} + H_{4pc} + H_{4p3d}, \tag{2.1}$$

where

$$H_{dp} = -\Delta \sum_{\boldsymbol{R},\sigma} d^\dagger_{\sigma\boldsymbol{R}} d_{\sigma\boldsymbol{R}} + T_{pp} \sum_{\langle r,r'\rangle,\sigma} (-1)^{\alpha_1} \left[p^\dagger_{\sigma r} p_{\sigma r'} + \text{H.c.}\right] + T_{pd} \sum_{\langle \boldsymbol{R},r\rangle,\sigma} (-1)^{\alpha_2} \left[d^\dagger_{\sigma\boldsymbol{R}} p_{\sigma r} + \text{H.c.}\right], \tag{2.2a}$$

$$H_{dd} = U_{dd} \sum_{\boldsymbol{R}} d^\dagger_{\uparrow\boldsymbol{R}} d_{\uparrow\boldsymbol{R}} d^\dagger_{\downarrow\boldsymbol{R}} d_{\downarrow\boldsymbol{R}}, \tag{2.2b}$$

$$H_{pp} = U_{pp} \sum_{r} p^\dagger_{\uparrow r} p_{\uparrow r} p^\dagger_{\downarrow r} p_{\downarrow r}, \tag{2.2c}$$

$$H_{\rm core} = \varepsilon_{1s} \sum_{\boldsymbol{R}} S^\dagger_{\boldsymbol{R}} S_{\boldsymbol{R}}, \tag{2.2d}$$

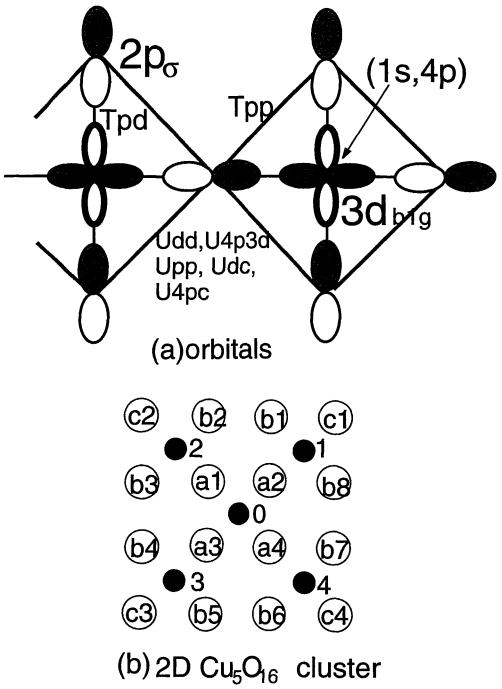

Fig. 4. Geometry of the system. (a) Orbitals in the model. O $2p_\sigma$ and Cu $\{1s,\ 3d(b_{1g}),\ 4p_\pi\}$ orbitals are taken into account. The blank (shaded) area of the ellipses represents positive (negative) phase. (b) Two-dimensional Cu_5O_{16} cluster with open boundary condition. The blank and closed circles represent oxygen and copper sites, respectively.

and

$$H_{dc} = U_{dc} \sum_{\boldsymbol{R}} \left[\sum_{\sigma} d^\dagger_{\sigma\boldsymbol{R}} d_{\sigma\boldsymbol{R}}\right] S_{\boldsymbol{R}} S^\dagger_{\boldsymbol{R}}. \tag{2.2e}$$

In these equations, $d^\dagger_{\sigma\boldsymbol{R}}$ creates a Cu $d_{x^2-y^2}$ *hole* with σ spin at $\boldsymbol{R}$ site and $p^\dagger_{\sigma r}$ creates a σ-bonded O $2p$ *hole* with σ spin at r site. Δ (> 0) is the charge-transfer (CT) energy between the p and d orbitals, and inter-site hopping energy T_{pp} and T_{pd} are related with the Slater-Koster parameters[11] as $T_{pp} = [(pp\pi) - (pp\sigma)]/2$ and $T_{pd} = \sqrt{3}(pd\sigma)/2$. The signs of T_{pp} and T_{pd} are described by α_1 and α_2, which are 0 or 1, depending on the relative position of a nearest-neighbor O-O and Cu-Cu pair, respectively. $S^\dagger_{\boldsymbol{R}}$ creates a Cu $1s$ *electron* at $\boldsymbol{R}$ site. U_{dd} and U_{dc} are on-site Cu $3d$-$3d$ and Cu $3d$-$1s$ Coulomb repulsion energies, respectively.

Generally, Cu $4p$ states are split off into a_2 ($4p_\pi$) and e ($4p_\sigma$) symmetries in terms of the local D_{4h} irreducible representations. For $4p$-$1s$ RXES of Nd_2CuO_4, however, both contributions are separable since there is no overlap between the experimental $4p_\pi$ and $4p_\sigma$ absorption threshold. We only take into account the $1s$-$4p_\pi$-$1s$ transition process. Then H_{4p} is given by

$$H_{4p} = \varepsilon_{4p\pi} \sum_{\boldsymbol{R}} Q^\dagger_{\boldsymbol{R}} Q_{\boldsymbol{R}} + t_0 \sum_{\langle \boldsymbol{R}.\boldsymbol{R}'\rangle} Q^\dagger_{\boldsymbol{R}} Q_{\boldsymbol{R}'}, \tag{2.2f}$$

where $Q^\dagger_{\boldsymbol{R}}$ creates a Cu $4p_\pi$ *electron* at $\boldsymbol{R}$ site, t_0 is $4p_\pi$-$4p_\pi$ nearest-neighbor hopping energy.

H_{4pc} and H_{4p3d} describe Cu $4p_\pi$-$1s$ and Cu $4p_\pi$-$3d$ intra-atomic interactions, respectively. The explicit forms are

$$H_{4pc} = -U_{4pc} \sum_{\boldsymbol{R}} Q^\dagger_{\boldsymbol{R}} Q_{\boldsymbol{R}} S_{\boldsymbol{R}} S^\dagger_{\boldsymbol{R}}, \tag{2.2g}$$

and

$$H_{4p3d} = -U_{4p3d} \sum_{\boldsymbol{R}} Q^\dagger_{\boldsymbol{R}} Q_{\boldsymbol{R}} \sum_{\sigma} d^\dagger_{\sigma\boldsymbol{R}} d_{\sigma\boldsymbol{R}}. \tag{2.2h}$$

In accordance with systematics of high-T_C compounds discussed by Ohta *et al.*[12] and with an *ab initio* calculation,[13] we set the valence electron parameters for large-cluster calculations of Nd_2CuO_4 as $\Delta = 2.5$, $T_{pd} = 1.21$, $T_{pp} = 0.55$ and $U_{dd} = 2U_{pp} = 8.8$ [eV]. A band calculation for Nd_2CuO_4[14] gave the $4p_\pi$ band width $W_\pi = 2.5$, thereby we estimate $t_0 = 0.3$ eV, along with one-electron formula of the band width $W_\pi = 8t_0$. U_{dc}, U_{4p3d} and U_{4pc} are set to be 7.5, 3.0 and 4.0 [eV].

In addition to the above model, we define an impurity Anderson model as the 2D extended d-p model whose $3d$ and $1s$ orbitals are all removed except for the central ones. Since the systems we are interested in have nominally d^9 configuration in the electron picture, the impurity problem is necessarily a one-hole problem with one electron in the $1s$ orbital or the $4p$ orbitals. In order to keep the main-satellite energy separation of XAS to be the same as that of the large cluster model, a different parameter $\Delta = 1.5$ eV is used for this model.[15]

2.2 Transition operators

As far as the $1s$-$4p_\pi$ absorption process is concerned,

the absorption operator T_1 is given by

$$T_1 = \sum_R e^{-ik_1 \cdot R} Q_R^\dagger S_R, \tag{2.3}$$

where k_1 is the wave vector of the incident photon. The emission operator T_2 is defined as $T_1^\dagger$ with the substitution of k_1 with k_2, which is the wave vector of the emitted photon. Then the transition operator of the $4p_\pi$-$1s$ RXES can be written as

$$T(z) = \sum_R S_R^\dagger Q_R G(z) Q_R^\dagger S_R, \tag{2.4}$$

where $G(z)$ is the resolvent operator defined as $G(z) = 1/(z - H)$, in which $z = E_g + \Omega - i\Gamma_m$, E_g and Ω being energies of the ground state and the incident photon, respectively. Γ_m is an energy width of the intermediate states, which is mainly due to the Auger decay process. We set $\Gamma_m = 0.8$ eV in the present calculations, considering semi-empirical data of the Auger process,[16] and another calculation of RXES for $3d$ systems.[17] In the above equation, we assume that $q \equiv k_2 - k_1$ is perpendicular to the CuO_2 plane in accordance with the experiment. Discussion on the polarization dependence[10] and the q dependence[18] of RXES will be published elsewhere.

Now we can construct spectral functions of XAS and RXES as

$$F_1(\Omega) = \sum_\mu |\langle \mu | T_1 | g \rangle|^2 \delta(\Omega + E_\mu - E_g), \tag{2.5}$$

and

$$F(\omega, \Omega) = \frac{1}{N} \sum_{f \neq g} |\langle f | T(z) | g \rangle|^2 \delta(\omega - \Omega + E_f - E_g), \tag{2.6}$$

where E_μ (E_f) is a final state energy of XAS (RXES), and ω denotes the emitted photon energy. N is the number of the Cu atoms. We concentrate our attention to the inelastic scattering in the present study.[5] For numerical calculations of the spectra we use the Lanczos method.[19]

§3. Analysis with Impurity Anderson Model

3.1 Properties of eigenstates

It is well-known that the eigenequation of the impurity Anderson model is exactly constructed as $x - \varepsilon_d = \Sigma_\star(x)$, where ε_d is unperturbed energy of the d orbital, and $\Sigma_\star(x)$ is the self-energy function:[20]

$$\Sigma_\star(x) = \frac{1}{N} \sum_{jk} \frac{|V_{jk}|^2}{x - \varepsilon_{jk} - i0}.$$

For the 2D periodic system with Cu-O distance a, there are two oxygen $2p$ bands:

$$\varepsilon_{jk} = \begin{cases} 4T_{pp} \sin(k_x a) \sin(k_y a), & j = 1 \\ -4T_{pp} \sin(k_x a) \sin(k_y a), & j = 2 \end{cases}.$$

For each band, the d-p hybridization energies are

$$V_{jk} = \begin{cases} -\sqrt{2} i T_{pd} [-\sin k_x a + \sin k_y a], & j = 1 \\ -\sqrt{2} i T_{pd} [\sin k_x a + \sin k_y a], & j = 2 \end{cases}.$$

The graphical representation of the eigenequation is depicted in Fig. 5. We see that a bound state g exists at -4.3 eV. This is the ground state $|g\rangle$. The above equation still holds for the intermediate state under substitution of ε_d with $\varepsilon_d + U_{dc} - U_{4p3d}$, as far as the energy dispersion of the $4p$ electron is neglected. In this case we have two bound states M and S, as described in the figure.

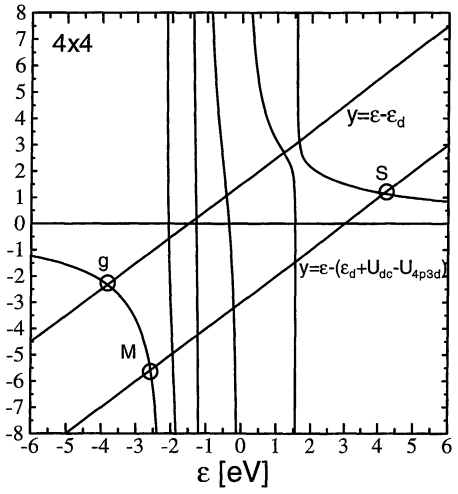

Fig. 5. Graphical representation of the eigenquations of the 2D impurity Anderson model with 4×4 oxygen network.

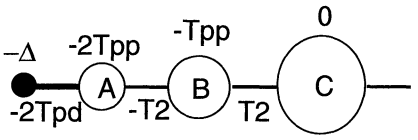

Fig. 6. A equivalent model of the 2D impurity Anderson model. The closed and open circles represent the impurity $3d$ orbital and O $2p$ molecular orbitals, respectively. The diagonal elements of the equivalent Hamiltonian are described above each of the circles. The hybridization matrix elements are described below each bond, where $T_1 = \sqrt{2} T_{pp}$ and $T_2 = \sqrt{2} T_{pd}$. Note that there happen to be degeneracies in molecular orbitals beyond C.

In order to study properties of the eigenstates further, we calculate partial density of states (PDOS) which is defined as

$$\rho_\phi(\varepsilon) = \sum_n |\langle \phi | \varepsilon_n \rangle|^2 \delta(\varepsilon - \varepsilon_n), \tag{3.1}$$

for a ϕ orbital. $|\varepsilon_n\rangle$ is an eigenstate of the system.

By constructing molecular orbitals with b_{1g} symmetry around the impurity site, it can be easily shown that the impurity Anderson model is equivalent to the model shown in Fig. 6. A is the nearest-neighbor orbitals to the Cu site, which is defined by

$$A^\dagger = \frac{1}{2}(-a_1^\dagger + a_2^\dagger + a_3^\dagger - a_4^\dagger). \tag{3.2}$$

Starting with this, we come to more accurate description of the whole system by taking B, C, ... molecular orbitals, where B and C are defined by

$$B^\dagger = \frac{1}{\sqrt{8}}(b_1^\dagger - b_2^\dagger + b_3^\dagger + b_4^\dagger - b_5^\dagger + b_6^\dagger - b_7^\dagger - b_8^\dagger), \tag{3.3}$$

and

$$C^\dagger = \frac{1}{2}(-c_1^\dagger + c_2^\dagger + c_3^\dagger - c_4^\dagger), \tag{3.4}$$

respectively. Since they span the complete set, note that a sum rule $\sum_\phi \rho_\phi = \rho$ as well as $\int d\varepsilon \rho_\phi = 1$ holds, ρ representing the total density of states (TDOS).

Figure 7(a) shows PDOS of $3d$ and the A, B and C orbitals as well as TDOS for RXES final state. We see that ρ_d and ρ_A have definite peaks at the ground state and at around 5.2 eV. The energy separation is approximately equal with the value obtained from the formula of the bonding-antibonding separation[15]

$$W = \sqrt{(-\Delta + 2T_{pp})^2 + 16T_{pd}^2}$$

in the simple CuO_4 cluster. This implies that the 5.2 eV peak corresponds to the antibonding state. Since these bonding and antibonding orbitals are just two ones in the simple CuO_4 cluster, the 5.2 eV excitation is nearly local, i.e. the hole spend most of its time at the plaquette with the impurity.[21]

On the other hand, we notice that the state at about 2 eV has little d and A weight. This means that it is a nearly pure p state, which has little amplitude at the impurity plaquette. In other words, it is a nonlocally excited state. This character makes a sharp contrast to the ground state and the 5.2 eV excited state, and it is directly reflected in the Ω dependence of RXES.

3.2 XAS

Figure 7(b) shows calculated Cu $1s$-$4p$ XAS and PDOS for the intermediate (XAS final) state. The energy dispersion of the $4p$ electron is neglected in the calculation of PDOS for simplicity, but it is fully included in that of XAS.

We see that the major weight of the main peak of XAS, which is denoted by $|M\rangle$ hereafter, lies on the A orbital. This is consistent with the standard notation $\underline{c}d^{10}\underline{L}$ in the electron picture, but there are no little weights in both d and B orbitals. The satellite peak of XAS, which is denoted by $|S\rangle$ hereafter, is composed mainly of the d orbital and slightly of the A orbital, being consistent with the standard notation $\underline{c}d^9$.

As seen from Fig. 7(a), $|g\rangle$ as the initial state of XAS consists of d and A orbitals approximately in the ratio of 5 : 5. Large weight in these orbitals is a necessary condition to have a strong intensity in XAS. Although $|M\rangle$ and $|S\rangle$ similarly fulfill this condition, Fig. 7(b) shows that their XAS intensities are quite different. The reason comes from a phase cancellation mechanism. Both $|g\rangle$ and $|M\rangle$ are split-off states at lower energy side of the continuum, while $|S\rangle$ is the split-off one at the opposite side. Thus we have considerable phase cancellation in the process $|g\rangle \to |S\rangle$.

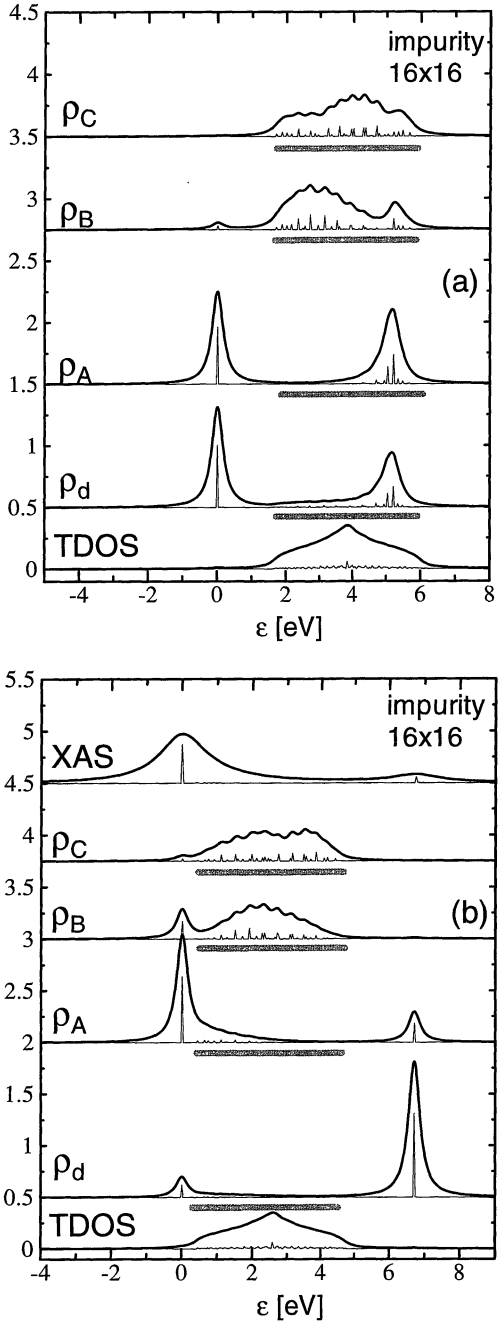

Fig. 7. (a) Total and partial densities of states of the impurity $3d$ orbital and O $2p$ molecular orbitals (A, B and C) defined in the text. TDOS and PDOS's are calculated with the impurity Anderson model with $N = 16 \times 16$ oxygen network, and they are convoluted with Lorentzian $\Gamma_L = 0.2$ eV (HWHM). All densities are normalized so that the integrated areas are to be unity. The shaded bars are guide to eye to represent unperturbed O $2p$ band width. (b) Total and partial densities of states (PDOS) in the *intermediate* state. The energy dispersion of the $4p$ electrons is disregarded for simplicity to calculate PDOS, but it is fully included to calculate XAS. Cu $1s$-$4p_\pi$ XAS are convoluted with $\Gamma_L = 0.8$ eV. The origin of the abscissa is adjusted to the ground state energy for both (a) and (b).

3.3 RXES

Calculated results of the Cu $4p_\pi$-$1s$ RXES are shown in Fig. 8, where CT excitations appear as inelastic spectra. The elastic peak is omitted from each spectrum.

Roughly speaking, we have broader spectra when Ω is tuned at M, while a single feature at around 5.2 eV appears for other Ω. As discussed in the preceding subsection, the value 5.2 eV is nearly the same as the bonding-antibonding separation in CuO_4 cluster. Within the present parameters, it is approximately given by $W \simeq 4T_{pd}$. The lowest position of the inelastic peak is estimated as the energy difference between the bottom of

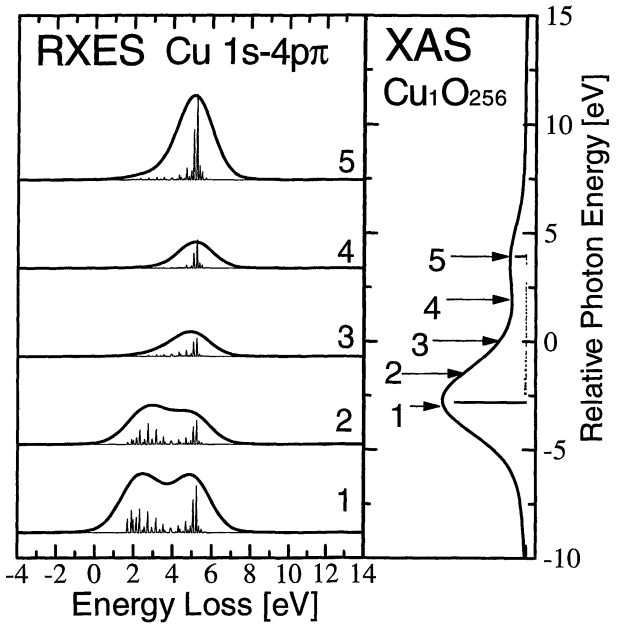

Fig. 8. Calculated Cu $4p_\pi$-$1s$ RXES and XAS spectra for Cu_1O_{256} cluster (impurity Anderson model). The arrows indicate the incident photon energies, and their numbers correspond to those in RXES.

the p band and the bonding state in CuO_4 cluster:

$$-4T_{pp} - \frac{1}{2}(-\Delta - 2T_{pp} - W) \simeq \frac{\Delta}{2} + 2T_{pd} - 3T_{pp}.$$

This formula gives a rough estimation of the CT gap from the viewpoint of the impurity Anderson model. Since it is believed that $(\Delta - 2T_{pp})$ is the same order of T_{pd} for high-T_c compounds, note that a naive estimation $\varepsilon_{\rm gap} \simeq \Delta$ which comes from the simple limit of weak d-p hybridization does not hold.

We now discuss the Ω dependence of RXES. First we consider the case when Ω is at $|S\rangle$. This intermediate state is strongly localized in the impurity plaquette, as shown in Fig. 7(b). Moreover, the phase of it matches the 5.2 eV excitation well by the aforementioned reason. Thus the main peak of RXES appears around 5.2 eV.

Second, $|M\rangle$ has not a little weight in extended orbitals such as B. Since $|M\rangle$ is much closer to the continuum than $|g\rangle$ in Fig. 5, it well hybridizes with p orbitals. The limit $U_{dc} \to \infty$ is helpful to illustrate the situation. The d hole is completely pushed out to the p bands in this case, naturally getting over the nearest-neighbor ligand orbital. In this sense, $|M\rangle$ as well as the 2 eV excitation has a nonlocal character, through which the transition from $|M\rangle$ to the states around 2 eV is caused. $|M\rangle$ has also large weight in A, so that the overlap with the 5.2 eV excitation is large, although there is no reason for the intensity enhancement by the phase matching in this case. This brings about the emission intensity around 5.2 eV, resulting in the broader spectra.

Finally, since the absorption intensity in the region between $|M\rangle$ and $|S\rangle$ is extremely small, spectral shapes of 2, 3 and 4 in Fig. 8 are basically determined by virtual transition process, although the 2 eV excitation is slightly favorable for these intermediate states which have large extended p weight.

3.4 Excitation energy dependence of the 5.2 eV intensity

Let us consider the mechanism of the Ω-dependence of the inelastic peak intensity around 5.2 eV. For the CuO_4 cluster, there are only two states in the final states of RXES. The intermediate states are also spanned in two-dimensional Hilbert space as far as the energy dispersion of $4p$ electron is disregarded, so that $|M\rangle\langle M| + |S\rangle\langle S| = 1$ holds. Since the line width Γ_m is much smaller than the energy separation between S and M, we have the following identity between transition amplitudes $|g\rangle \to |5.2\rangle$ through M and S intermediate states:

$$\langle 5.2|T_2|M\rangle \frac{1}{\mathrm{i}\Gamma_m}\langle M|T_1|g\rangle + \langle 5.2|T_2|S\rangle \frac{1}{\mathrm{i}\Gamma_m}\langle S|T_1|g\rangle$$
$$= \frac{1}{\mathrm{i}\Gamma_m}\langle 5.2|T_2T_1|g\rangle = \frac{1}{\mathrm{i}\Gamma_m}\langle 5.2|g\rangle = 0,$$

which demonstrates that the two amplitudes are the same except for their signs, and thus the Ω-scan of the 5.2 eV intensity takes a symmetric "U-shape". We then take its asymmetry as a measure of nonlocal nature of excitations.

The Ω-scan is plotted in Fig. 3(a) with the dashed curve.[22] It shows that the scan takes almost the U-shape, and that the large-cluster effect with respect to O $2p$ band plays a minor role. It suggests that the transition process which gives the 5.2 eV excitation as a final state of RXES is mainly controlled by local orbitals such as d and A.

Recently Nakazawa *et al.*[23] pointed out the importance of configuration dependence[24] of cation-ligand hybridization in Ce $4f$-$3d$ RXES of CeO_2. In order to see the effect, we here introduce a parameter R_c, which renormalizes T_{pd} of the plaquette with the core hole as $R_c \times T_{pd}$ in the *intermediate* (XAS final) states.

The calculated results with $R_c = 0.8$ are also given in Fig. 3(a) (solid curve). All calculated scans are normalized so that each height of the maximum peak is the same. We see that $R_c \neq 1$ suppresses the 5.2 eV intensity (although the suppression is too small to reproduce the experimental result) when Ω is tuned around $|M\rangle$, and strengthens its asymmetry. The limit of $R_c \to 0$ helps to make the situation clear. Since the main peak of XAS has no d weight in this case, and since the orbital A is not stabilized through d-p hybridization, the extra p weight contained in the extended B, C, ... orbitals necessarily comes into the state to reduce the large A weight. Also for a finite R_c, it must work to increase the extended weight in $|M\rangle$. Thus overlap between $|M\rangle$ and the 5.2 eV excitation tends to be decreased by R_c in comparison with that of $|S\rangle$. This is the explanation of the asymmetric shape of the Ω-scan of the 5.2 eV intensity.

Although the calculated XAS with the impurity Anderson model well reproduces the experimental main-satellite separation, there are considerable discrepancies with experimental data in the Ω-scan of the 5.2 eV intensity. When Ω is tuned at the main peak of XAS, the 5.2 eV intensity always exhibits one of the two peaks of the U-shape as far as the impurity Anderson model is used. The observed suppression effect can not be reproduced at all. This is nothing but an indication of a

nonlocal effect (which is brought about by Zhang-Rice singlet formation) in the intermediate states of multi-Cu clusters, beyond the simple O $2p$ band effects. It will be discussed in the next section in detail.

§4. Analysis with Multi-Cu Models

4.1 Properties of eigenstates

Considering the results with the impurity Anderson model and the experimental fact that an antiferromagnetic order of d holes is realized in $|g\rangle$. we are led to an idea that eigenstates of a multi-Cu cluster model are described as some superposition of those of each plaquette.[25] We expect that there are relatively local excitations around 5.2 eV, but somewhat new states should be created around 2 eV above $|g\rangle$ upon going from the impurity to the multi-Cu model.

In order to see the point in detail, we again calculate PDOS and TDOS for a Cu_3O_{10} cluster with Householder method,[26] based on the fact that spectra of Cu_3O_{10} are essentially the same as that of Cu_5O_{16}. We choose

$$|\mathrm{AF}\rangle = d^\dagger_{1\uparrow} d^\dagger_{2\uparrow} d^\dagger_{0\downarrow} |\mathrm{vacuum}\rangle,$$

as a counterpart of $|d\rangle$ in the impurity model, and

$$|A'\rangle = L^\dagger_{0\downarrow} d_{0\downarrow} |\mathrm{AF}\rangle,$$

as a counterpart of $|A\rangle$, where the suffix 0 means the central site, and $L^\dagger_{0\downarrow}$ is the creation operator of its nearest-neighbor ligand orbital with local b_{1g} symmetry of the local D_{4h} group, just as eq. (3.2). The numbering rule is given in the inset of Fig. 9(a).

In addition to these, we define also $|B'\rangle = B^\dagger_{0\downarrow} d_{0\downarrow} |\mathrm{AF}\rangle$ and $|C'\rangle = C^\dagger_{0\downarrow} d_{0\downarrow} |\mathrm{AF}\rangle$, where $B^\dagger_{0\sigma}$ and $C^\dagger_{0\sigma}$ are defined by

$$B^\dagger_{0\sigma} = \frac{1}{2}(b^\dagger_{1\sigma} - b^\dagger_{2\sigma} + b^\dagger_{3\sigma} - b^\dagger_{4\sigma}), \tag{4.1}$$

and

$$C^\dagger_{0\sigma} = \frac{1}{\sqrt{2}}(c^\dagger_{1\sigma} - c^\dagger_{2\sigma}), \tag{4.2}$$

respectively. The orbitals $L^\dagger_{0\sigma}$, $B^\dagger_{0\sigma}$ and $C^\dagger_{0\sigma}$ have a_g symmetry in terms of the D_{2h} irreducible representation of the Cu_3O_{10} cluster, so that all the above states have the same symmetry (B_{3u}) as the ground state.

The result of the final state is shown in Fig. 9(a) within the energy range corresponding to the one-hole CT excitation ($E - E_g$ less than about 7 eV). We see that ρ_{AF} and $\rho_{A'}$ have definite structures at the ground state and at 5.5 eV. These features are similarly observed in Fig. 7. We thus conclude that the 5.5 eV excitation is nearly localized in each plaquette, i.e. "intra-plaquette" excitation.

There are also some structures in the energy region between $|g\rangle$ and the 5.5 eV excitation, which are not observed in Fig. 7. A detailed calculation shows that the peak g_1 has large overlap with states which have frustrated d-spin arrangements such as

$$\frac{1}{\sqrt{N_u}} \sum_{i=1}^{N_u} (-1)^{\alpha_i} d^\dagger_{i\downarrow} d_{i\uparrow} d^\dagger_{0\uparrow} d_{0\downarrow} |\mathrm{AF}\rangle,$$

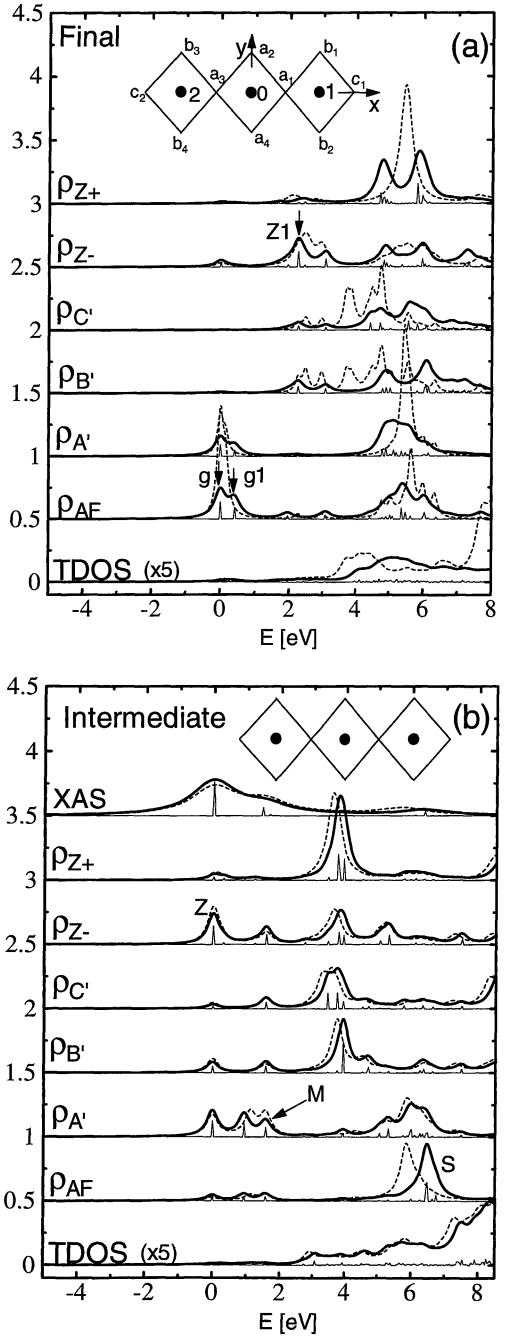

Fig. 9. (a) Total and partial densities of states in RXES final state for Cu_3O_{10} cluster, whose structures are shown in the panel. The definition of the state $|\mathrm{AF}\rangle$ and so on is given in the text. The solid and dashed curves represent the results with $T_{pp} = 0.55$ and 0, respectively. (b) TDOS and PDOS in the intermediate (XAS final) state. Cu $1s$-$4p_\pi$ XAS is also shown. The energy dispersion of the $4p$ electron is disregarded to calculate PDOS, but fully included to calculate XAS. The solid and dashed curves are obtained with $R_c = 1.0$ and 0.8, respectively. For both (a) and (b), the origin of the abscissa is adjusted to be the lowest state energy, and all spectra are broadened with Lorentzian ($\Gamma_L = 0.2$ eV), whose integrated areas are normalized to be unity.

where N_u is the number of up-spin hole, and α_i is determined so that the state is the B_{3u} representation of the overall symmetry group D_{2h}. Thus we conclude that the peak is due to spin excitations.

Figure 9(a) also shows PDOS's and TDOS of $T_{pp} = 0$ with the dashed curves. It is observed that a few peaks

between 2 and 3 eV survive with slight energy shifts. Since the impurity Anderson model is reduced to the CuO_4 cluster in this limit, we conclude that the existence of d-p network particular to multi-Cu models is their origin. In order to study the properties of these peaks we here define a new PDOS for

$$|Z\pm\rangle = \frac{1}{\sqrt{2}}(z^\dagger_{1\pm}d_{1\uparrow} + z^\dagger_{2\pm}d_{2\uparrow})d_{0\downarrow}|\mathrm{AF}\rangle, \tag{4.3}$$

where the operator $z^\dagger_{i\pm}$ is defined by

$$z^\dagger_{i\pm} = \frac{1}{\sqrt{2}}(d^\dagger_{i\uparrow}L^\dagger_{i\downarrow} \pm d^\dagger_{i\downarrow}L^\dagger_{i\uparrow}). \tag{4.4}$$

$|Z-\rangle$ ($|Z+\rangle$) describes a state where a hole pushed out from the central plaquette forms a local singlet (triplet) at the nearest-neighboring plaquettes. The phase factor in eq. (4.3) was determined so that its global symmetry is in agreement with that of the ground state (B_{3u}).

According to the calculated result, ρ_{Z-} has clear structure (Z_1) between 2 and 3 eV, but little weight in ρ_{Z+}. Although the impurity Anderson model contains the nearly pure p states in this energy range, this result suggests that *the CT excitation in this energy range has ZR singlet like character.* Hence the CT gap may be defined by the energy to move a hole from the bonding orbital at a plaquette to the surroundings, forming the local singlet. If $2T_{pd} \ll \Delta$ held as Zhang and Rice originally discussed,[9] the binding energy of the local singlet would be estimated by their formula $-8T^2_{pd}[1/\Delta^2 + 1/(U_{dd} - \Delta)^2]$. But our parameter gives $2T_{pd} \simeq \Delta$. We hence obtain the conclusion again that the simple estimation that $\varepsilon_{\mathrm{gap}} \simeq \Delta$ does not hold. We will give more detailed discussion elsewhere on this subject through an analysis of Cu $4p$-$1s$ RXES of $CuGeO_3$, which has relatively larger Δ.[27,28]

Except for this fact, PDOS's in Figs. 7 and 9 have much in common. For example, the 2 eV excitation has hardly AF weight, but has relatively large weight in $\rho_{B'}$ and $\rho_{C'}$.

Similar arguments are applicable to the intermediate state. The calculated results are given in Fig. 9(b) for the system with a core hole at the central site. The energy dispersion of $4p$ electron is neglected to calculate PDOS. It is clearly shown that AF weight is transferred to about 6.6 eV higher than the lowest energy state, being denoted by "S". Naturally, the main structure in ρ_{AF} corresponds to $\underline{c}d^9$ in the standard notation of the impurity Anderson model.

In addition, first, we can assign the lowest energy feature "Z" to the state with the local singlet (*not* triplet). This is the direct evidence of appearance of the ZR singlet in the intermediate state, also in the final state of $2p$-XPS first discussed by van Veenendaal *et al.*,[15] i.e. a hole pushed out by the corehole potential moves to the neighboring plaquettes to form the local singlet. Second, structures about 1.5 eV above the ZR state is attributed to a charge-transferred state having a considerable weight in the nearest-neighbor orbital of the core hole site, corresponding to $|M\rangle$ of the impurity Anderson model.

Figure 9(b) also shows Cu $1s$-$4p_\pi$ XAS. In contrast to the impurity Anderson model, there are three structures in XAS, which are the above discussed Z, M and S. This interpretation has close relationship with that of $2p$-XPS.[15,29]

4.2 RXES

Figure 10 shows XAS and RXES spectra with the Cu_5O_{16} cluster with open boundary condition. Calculated spike spectra of RXES are convoluted with Gaussian $\Gamma_G = 0.95$ eV (HWHM) in accordance with the experimental resolution.[6] XAS is also broadened with Lorentzian $\Gamma_L = 0.8$ to take the lifetime effect into account and $\Gamma_G = 0.8$ eV to reproduce the experimental peak width. To avoid boundary effects the core hole is fixed to the central site for both RXES and XAS. Effects of spatial coherence are discussed separately elsewhere in the context of momentum-transfer dependence.[18]

As is the case of the impurity Anderson model, RXES in Fig. 10 have two structures around 2 and 5.7 eV, which are hereafter symbolically denoted by $|2\rangle$ and $|5.7\rangle$, respectively. The latter value is somewhat larger than that of the impurity and Cu_3O_{10} models, but closer to the experimental value.

The 2 eV intensity is considerably enhanced when the incident photon energy Ω is tuned at the main peak "1" of XAS. This is observed in common in the case of the impurity Anderson model, but the enhancement is extremely intense in this case. The reason is that both 2 eV excitation and the main absorption peak have a ZR singlet, so that their overlap is very large.

On the other hand, since $|5.7\rangle$ is the intra-plaquette excitation, corresponding to the 5.5 eV excitation of Cu_3O_{10} cluster discussed in the preceding subsection, the overlap with the ZR state is expected to be quite small. Because the ZR state contains a plaquette with almost

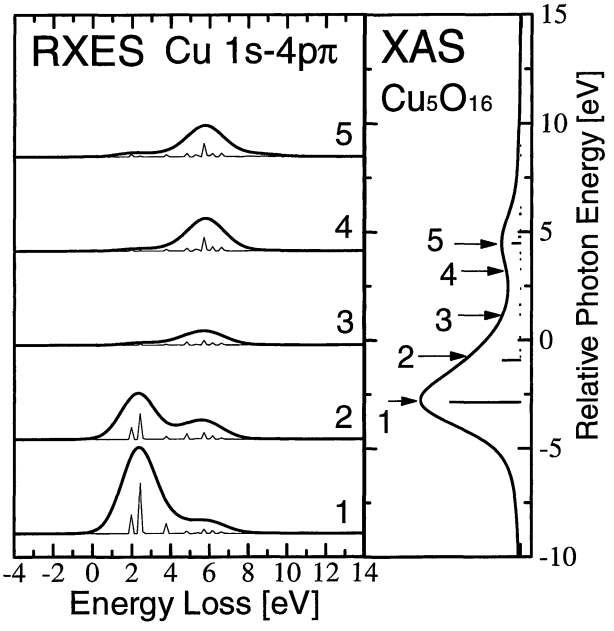

Fig. 10. Calculated Cu $4p_\pi$-$1s$ RXES and XAS spectra with Cu_5O_{16} cluster model. The core hole is fixed to the central site in order to avoid boundary effects. The arrows marked with numbers in XAS indicate incident photon energies, and the numbers in RXES represent the corresponding excitation energies.

no hole. As a result, the 5.7 eV intensity is suppressed when Ω is tuned at the XAS main peak. We believe that this is the basic mechanism of the experimental suppression effect.

Since the satellite peak "5" has the AF weight as the dominant component as shown in Fig. 9(b), it is expected to have large overlap with $|5.7\rangle$: both are almost localized at each plaquette. This coupling would be preferred also from the phase matching point of view. Also it is expected to have little overlap with the 2 eV excitation containing the ZR singlet like state. Thus the RXES spectrum has an only structure around the 5.7 eV excitation.

When Ω is tuned at the shoulder "2", which was denoted by M in the preceding subsection, the situation is halfway. The dominant weight of M lies on $|A'\rangle$, but more extended orbitals have no negligible weight as shown in Fig. 9(b), so that the former gives rise to the intensity of the 5.7 eV excitation, and the latter causes the transition to the 2 eV excitation, resulting somewhat broader spectra.

4.3 Excitation energy dependence of the 5.7 eV intensity

The disagreement with the experimental data in the Ω-scan of the 5.2 eV intensity with the impurity Anderson model is essentially cleared up by taking the above multi-Cu effects into account. Calculated Ω-scans of the 6 eV (actually 5.7 eV) intensity in $4p_\pi$-$1s$ RXES of Nd_2CuO_4 are given in Fig. 3(b), where the results with $R_c = 1$ and 0.8 are represented with the dashed and thick solid curves, respectively.

In contrast to the double peaked shape of the impurity model calculation, the multi-Cu one gives a three-peaked structure. As a result of the suppression effect for Ω tuned at around -3 eV, it reproduces the experimental data much better than the impurity one.

Introducing R_c, we see that the 5.7 eV intensity is more suppressed when Ω is tuned at the main peak (Z), but enhanced when Ω is tuned at the shoulder (M), improving the agreement with the experiment. TDOS and PDOS's with $R_c = 0.8$ for Cu_3O_{10} cluster is shown in Fig. 9(b) with the dashed curve. We see that, first, ρ_{Z-} is enhanced by $R_c \neq 1$ at the lowest state "Z". This means that the hole is pushed out from the core hole plaquette more strongly, so that the overlap with the intra-plaquette excitation tends to be decreased. On the other hand, $\rho_{A'}$ is increased around the energy of the shoulder "M", being consistent with the discussion in the subsection 3.4. However $\rho_{B'}$ and $\rho_{C'}$ are decreased at this energy, so that the overlap with the intra-plaquette excitation tends to be increased. This means that the existence of the ZR singlet state reduces extended nature of the state M.

We finally give a few comments on the present study. There is slight discrepancy with the experimental data mainly due to the incompleteness of the suppression effect. We have performed the calculations with relatively small clusters such as Cu_3O_{10} or Cu_5O_{16}. All excitations necessarily have more or less local character as far as the system is finite. Moreover, it is impossible to avoid boundary effects perfectly. Since we believe that the origin of the suppression effect is the nonlocal charge-transfer to form the ZR singlet, it is expected that the finite size effect plays some role. In order to make the point clear, detailed experimental and theoretical analysis is needed for one-dimensional systems,[30] where we can extend the cluster size without facing the limitation of the memory size of computers.

In addition, our recent calculation on the q-dependence of $4p$-$1s$ RXES of Sr_2CuO_3 shows that $|2\rangle$ is strongly q-dependent, i.e. nonlocal, while $|5.7\rangle$ has little q-dependence.[18] These results are consistent with the preceding discussions, and detailed discussion will be given in another paper.

§5. Concluding Remarks

We theoretically investigated the Cu $4p_\pi$-$1s$ RXES of Nd_2CuO_4 firstly with the impurity Anderson model. Utilizing PDOS functions, we found that excitations about 5.2 eV above the ground state have considerably localized character, and that excitations about 2 eV above the ground state are nearly pure p states, having less amplitude at the plaquette with the impurity.

In the large cluster calculations, however, the low energy excitations created by CT processes have ZR singlet like character in contrast to the result with the impurity Anderson model, although excitations about 5.7 eV above the ground state is similarly local ("intra-plaquette"). This difference is clearly reflected in the RXES spectra when the main absorption peak is resonated.

A conspicuous disagreement with the experimental 6 eV intensity as a function of the incident photon energy could not be removed with the impurity Anderson model. It was demonstrated that the difficulty is solved by taking Zhang-Rice singlet formation into account, using the multi-Cu model.

We finally discussed the role of the configuration dependence of d-p transfer. The satisfactory agreement with the experimental data is obtained with the large cluster calculation with R_c.

Although the present calculations have done for the undoped system, RXES would give direct and clear information of electronic structure of doped systems. Together with the q-dependence of RXES, this point is discussed elswhere.

Acknowledgements

We wish to thank J. P. Hill, C.-C. Kao and K. Hämäläinen for sending us their experimental data and for their discussions. The early stage of this work was done by M. Matsubara. We thank M. Matsubara and K. Okada for their valuable discussions. This work is partly supported by a Grant-in-Aid for Scientific Research from the Ministry of Education, Science, Sports and Culture. The computation in this work was done using the facilities of the Super-Computer Center, Institute for Solid State Physics, the University of Tokyo.

1) Y. Tezuka, S. Shin, A. Agui, M. Fujisawa and T. Ishii: J.

Phys. Soc. Jpn. **65** (1996) 312.
2) S. M. Butorin, J.-H. Guo, M. Magunuson and J. Nordgren: Phys. Rev. B **55** (1997) 4242.
3) S. M. Butorin, J.-H. Guo, M. Magunuson, P. Kuiper and J. Nordgren: Phys. Rev. B **54** (1996) 4405.
4) C. C. Kao, W. A. L. Caliebe, J. B. Hastings and J.-M. Gillet: Phys. Rev. B **54** (1996) 16361.
5) T. Idé and A. Kotani: J. Phys. Soc. Jpn. **67** (1998) 3621.
6) J. P. Hill, C.-C. Kao, W. A. L. Caliebe, M. Matsubara, A. Kotani, J. L. Peng and R. L. Greene: Phys. Rev. Lett. **80** (1998) 4967.
7) Y. Tokura, H. Takagi and S. Uchida: Nature (London) **337** (1989) 345; H. Takagi, S. Uchida and Y. Tokura: Phys. Rev. Lett. **62** (1989) 1197.
8) R. J. Gooding, K. J. E. Vos and P. W. Leung: Phys. Rev. B **50** (1994) 12866.
9) F. C. Zhang and T. M. Rice: Phys. Rev. B **37** (1988) 3578.
10) K. Hämäläinen, J. P. Hill, S. Huotari, C.-C. Kao, L. E. Berman, A. Kotani, T. Idé, J. L. Peng and R. L. Greene: in preparation.
11) J. C. Slater and G. F. Koster: Phys. Rev. **94** (1954) 1498.
12) Y. Ohta, T. Tohyama and S. Maekawa: Phys. Rev. B **43** (1991) 2968.
13) A. K. McMahan, R. M. Martin and S. Satpathy: Phys. Rev. B **38** (1988) 6650.
14) S. Matsuno and H. Kamimura: J. Superconductivity **7** (1994) 517.
15) M. A. van Veenendaal, H. Eskes and G. A. Sawatzky: Phys. Rev. B **47** (1993) 11462.
16) M. O. Krause and J. H. Oliver: J. Phys. Chem. Ref. Data, **8** (1979) 329.
17) M. Taguchi, T. Uozumi and A. Kotani: J. Phys. Soc. Jpn. **66** (1996) 247.
18) T. Idé and A. Kotani: in preparation; Meeting abstracts of the Physical Society of Japan **54** (1999) Issue 1, Pt. 2, p. 191.
19) For a review article, see, E. Dagotto: Rev. Mod. Phys. **66** (1994) 763.
20) G. D. Mahan: *Many-Particle Physics* (Plenum Press, New York, 1990) Chap. 4.
21) More exactly, this excitation energy, which corresponds to the experimental value 6 eV, depends on the model, and takes 5.2 eV for the impurity Anderson model, 5.5 eV for Cu_3O_{10} cluster model and 5.7 eV for Cu_5O_{16} cluster model.
22) The present result is essentially the same as that given in ref. 6 with an impurity Anderson model, but quantitatively they are slightly different because of a slightly different O $2p$ band model and slightly different parameter values.
23) M. Nakazawa, S. Tanaka, T. Uozumi and A. Kotani: J. Phys. Soc. Jpn. **65** (1996) 2303.
24) O. Gunnarsson and O. Jepsen: Phys. Rev. B **38** (1988) 3568.
25) J. H. Jefferson, H. Eskes and L. F. Feiner: Phys. Rev. B **45** (1992) 7959.
26) W. H. Press, B. P. Flannery, S. A. Teukolsky and W. T. Vetterling: *Numerical Recipes* (Cambridge University Press, 1989) Chap. 11.
27) F. Parmigiani, L. Sangaletti, A. Goldnoi, U. del Pennino, C. Kim, Z.-X. Shen, A. Revcolevschi and G. Dhalènne: Phys. Rev. B **55** (1997) 1459.
28) Y. Mizuno, T. Tohyama, S. Maekawa, T. Osafune, N. Motoyama, H. Eisaki and S. Uchida: Phys. Rev. B **57** (1998) 5326.
29) K. Okada and A. Kotani: Phys. Rev. B **52** (1995) 4794.
30) K. Okada, A. Kotani, K. Maiti and D. D. Sarma: J. Phys. Soc. Jpn. **65** (1996) 1844.